ACS Partner Journal

ENVIRONMENT & HEALTH

Open Access

pubs.acs.org/EnvHealth

Article

Exposure to Manganese Induces Autophagy−Lysosomal Pathway Dysfunction-Mediated Tauopathy by Activating the cGAS−STING Pathway in the Brain

Xin Zhang, Jingjing Liu, Shiyin Zhong, Zhimin Zhang, Qiongli Zhou, Jirui Yang, Xuhong Chang, and Hui Wang*

Cite This: *Environ. Health* 2025, 3, 199−212

Read Online

ACCESS | Metrics & More | Article Recommendations

ABSTRACT: Manganese (Mn) exposure leads to pathological accumulation of Tau-associated neurodegenerative disease and has become a major public health concern. However, the precise mechanism underlying this effect remains unclear. Here, the mechanism by which Mn induces dysfunction of autophagy−lysosomal pathway-mediated tauopathy by activating the cGAS−STING pathway was explored both *in vitro* and *in vivo*. Mn exposure induced tauopathy in microglia and in mice while activating the cGAS−STING pathway, inducing type I interferon production, and impairing the degradation function of the autophagy−lysosomal pathway. Importantly, inactivation of the cGAS−STING pathway rescued the degradation activity of the autophagy−lysosomal pathway, while tauopathy was markedly attenuated, as shown in both *cGAS*-knockout and *STING*-knockout BV2 microglia and in mice. Moreover, the autophagy inhibitor 3-methyladenine (3-MA) restored the impaired degradation activity of the autophagy−lysosomal pathway by inactivating the cGAS−STING pathway, thereby clearing Tau aggregation. Taken together, these results indicate that Mn exposure induces tauopathy by impairing the function of the autophagy−lysosomal pathway through the activation of the cGAS−STING pathway. Thus, this study identifies a novel mechanism by which Mn exposure induces Tau aggregation, which in turn triggers potential neurotoxicity, providing a foundation for future drug target research.

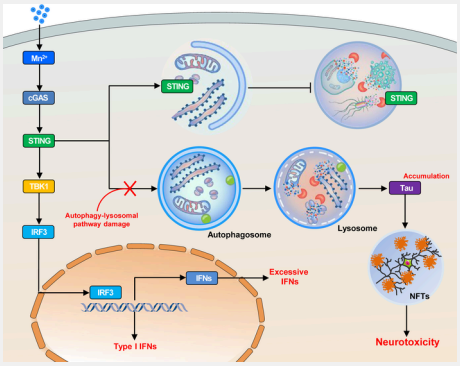

KEYWORDS: *manganese, Tau, autophagy, cGAS−STING pathway*

1. INTRODUCTION

Neurodegenerative diseases (NDDs), such as Alzheimer's disease (AD) and Parkinson's disease (PD), are caused by structural and functional changes in neural networks and the loss of neurons in the central nervous system (CNS) or peripheral nervous system (PNS) and affect the lives of millions of people worldwide.[1] Increased deposition of Tau, amyloid-β (Aβ) plaques, α-synuclein and other characteristic proteins is the key pathological hallmark of a variety of NDDs.[1,2] The risk for NDDs is attributable to genetic and environmental factors.[3] Various environmental factors play crucial roles in the etiology of NDDs. Metallic elements are widespread and persistent in the environment. Metallic elements such as manganese (Mn), cadmium (Cd), and lead (Pb) are well documented potentially neurotoxicants that are associated with impaired cognitive function and cognitive decline, and are potential factors in the development of canonical AD and PD pathologies.[4,5]

Mn is an essential trace element for humans and plays a crucial role in regulating a variety of biological processes at normal concentrations. It is also an emerging pollutant due to its wide application in industry and agriculture.[6] Mn is a major pollutant in mine wastewater and an important environmental challenge globally.[7] The main removal mechanism of Mn in mine wastewater is adsorption and redox precipitation. However, Mn removal is generally more challenging due to its complex chemistry.[7] Mn overload in the environment poses a major threat to human health.[8,9] For decades, environmental and occupational exposure to Mn has been associated with neurological effects.[10] Excess Mn deposited mainly in the brain, causing potentially neurotoxic symptoms of movement disorders and cognitive deficits, known as manganism.[11−13] Epidemiological data have shown that long-term excessive exposure to Mn can significantly reduce the learning ability and intelligence level of children,[14] and environmental air Mn

Received: September 5, 2024
Revised: November 5, 2024
Accepted: November 7, 2024
Published: November 12, 2024

https://doi.org/10.1021/envhealth.4c00176
Environ. Health 2025, 3, 199−212

exposures of ≥203 ng/m^3 are associated with cognitive dysfunction, depression and anxiety.[15,16] There have been recurring reports of Mn contamination in groundwater, and there is growing evidence that oral Mn intake is associated with neurotoxicity.[17,18] Neurotoxicity caused by excessive Mn exposure is associated with the risk of neurodevelopmental impairment and the development of NDDs, such as AD, PD, and attention-deficit hyperactivity disorder (ADHD),[13,19−21] which is a global public health issue that has gained increasing public concern.[22] Recent findings suggest that excessive Mn exposure is a contributing factor for sarcopenia and that inflammation mediates this relationship.[23] In view of the hazards of Mn, the World Health Organization (WHO) estimates that the systemic Mn absorption rate of healthy Western adults is 180 μg/d.[24] A Mn content greater than 40 μg/L is considered a medium−high exposure concentration that can lead to chronic manganism.[24] A biological reference value of 15 μg/L Mn in blood has been established in Germany.[24] The mechanisms of Mn-induced potentially neurotoxicity, including oxidative stress, reactive oxygen species (ROS) formation, mitochondrial dysfunction, protein aggregation, neuroinflammation, and ferroptosis, have been extensively investigated in recent decades.[25−27] However, the exact pathogenic mechanism(s) of Mn are still poorly understood.

The cyclic GMP−AMP synthase (cGAS)−stimulator of interferon gene (STING) pathway has been identified as the major DNA receptor pathway, which activates the innate immune response by recognizing heterologous DNA and inducing type I interferon (IFN-I) expression in mammalian cells.[28,29] The cGAS−STING pathway not only mediates protective immune defense against cellular damage and DNA-containing pathogens,[30] but also drives deleterious IFN-I activation in NDDs,[31,32] and exacerbates Aβ pathology.[33] Emerging evidence has shown that Mn^{2+} is the second most efficient activator of the cGAS−STING pathway and is completely independent of double-stranded DNA (dsDNA).[34−36] However, the role of the cGAS−STING pathway in the neurotoxicity induced by Mn exposure remains unclear.

Tau pathology is closely related to synaptic loss, neurodegeneration and cognitive decline. The pathological accumulation and spread of the Tau protein are key features of the NDDs known as tauopathies.[37,38] Oligomers, misfolded Tau, and phosphorylated Tau species have been found at synaptic terminals in AD brains, and Tau pathology may progress via transsynaptic spread.[39] The activation of microglia is involved in Tau-mediated pathobiology, which is a prominent pathological feature in tauopathies.[40,41] Tau is a major therapeutic target for NDDs, and currently, eliminating or inhibiting Tau aggregates in the brain is a strategy to prevent and treat NDDs.[42−45] Thus, pharmacological approaches aimed at reducing Mn-induced Tau expression may provide neuroprotection.

Autophagy is a process by which cells use lysosomes to selectively remove damaged and senescent organelles or degrade excess biological macromolecules. The ubiquitin−proteasome and autophagy−lysosomal pathways are associated with Tau clearance.[46] However, in Tau pathology, proteasomal dysfunction occurs so that it cannot be effectively degraded by the ubiquitin−proteasome system.[47] Therefore, it is necessary to activate the autophagy−lysosomal pathway to complete the degradation and clearance of abnormally aggregated Tau.

In the present study, we hypothesized that Mn exposure impaired Tau degradation via the autophagy−lysosomal pathway by activating the cGAS−STING pathway. This process ultimately leads to Tau accumulation in the brain, which in turn triggers potential neurotoxicity. We first observed that Mn exposure activated the cGAS−STING pathway, which induced Tau aggregation. Next, we evaluated the effects of Mn exposure that led to dysfunction of the autophagy−lysosomal pathway. And we explored the cGAS−STING pathway-mediated dysfunction of the autophagy−lysosome pathway and Tau expression. In addition, inhibition of the cGAS−STING pathway by autophagy inhibitors alleviated Mn-induced Tau aggregation. Therefore, this study not only reveals a new biological mechanism of Mn neurotoxicity but also provides novel potential targets for the treatment of NDDs caused by Mn exposure.

2. METHODS

2.1. Cell Lines and Cell Culture

BV2 microglia were purchased from Cyagen Bioscience, Inc. (Guangzhou, China). The cells were cultured at 37 °C with 5% CO_2 in RPMI 1640 (VivaCell, Shanghai, China) supplemented with 1% penicillin−streptomycin solution (Biological Industries, Israel) and 10% fetal bovine serum (FBS, Biological Industries, Israel). BV2 microglia were serially passaged once the plates reached 80−90% confluency.

Clustered regularly interspaced short palindromic repeats (CRISPR)/Cas9-mediated genome engineering was used to create *cGAS* (*Mb21d1*) and *STING* (*Tmem173*) gene knockout cell models. The sgRNA plasmids specifically targeting mouse *cGAS* and *STING* were purchased from Cyagen Biosciences, Inc. Plasmids containing each target sgRNA sequence were transfected into BV2 cells. Puromycin was added to screen the cells after transfection for 24−48 h. After 2−4 weeks, single clones were screened, and selected *cGAS*- and *STING*-knockout clones were validated by PCR (polymerase chain reaction) and sequencing to obtain the BV2$^{cGAS-/-}$ and BV2$^{STING-/-}$ cell lines. The sgRNA sequence for *cGAS* is 5′-CGGGCCGCAGCTTTCCGCGT GGG-3′, and the sgRNA sequence for *STING* is 5′-GTGGATCCTTTGCCACCCAAAGG-3′.

The BV2, BV2$^{cGAS-/-}$, and BV2$^{STING-/-}$ cell lines were cultured and expanded in serum-containing medium to ensure stable growth. The viability of these cell lines exposed to different concentrations of Mn^{2+} (0−400 μmol/L) under serum-free conditions for different durations (6, 12, and 24 h) was assessed using the cell counting kit-8 (CCK-8) (Apexbio, USA). In short, 96-well plates were used to seed the cells at a density of 1 × 10^4 cells/well. The cells were treated with the indicated concentrations of manganese chloride ($MnCl_2{\cdot}4H_2O$, Sigma, USA) for 24 h and then incubated with CCK-8 reagent for 3 h at 37 °C. The absorbance was determined using a microplate reader (Bio-Rad, USA) at 450 nm. The percentage of viable cells is equal to the ratio of the optical density (OD) between the treated group and the control group. 3-Methyladenine (3-MA) (Selleck, USA) at 10 μmol/L for 12 h was used to block autophagy in BV2 cells and assessed by CCK-8 assay.

2.2. Animal Studies

A total of 20 wild-type (WT) C57BL/6J mice were purchased from Lanzhou Veterinary Research Institute, Chinese Academy of Agricultural Sciences. The mice were housed under specific pathogen free (SPF) conditions in the Laboratory Animal Center of Lanzhou University under standard conditions of temperature (20 ± 3 °C), relative humidity (40−60%) and a 12 h light-dark cycle, and pelleted rodent food and filtered water were provided *ad libitum*. After 7 days of adaptive feeding, the mice were randomly divided into two groups: WT and WT+Mn, with 10 mice per group. The establishment of the Mn exposure mouse model and the collection of biological samples were performed as described in our previous publication.[48] In brief,

https://doi.org/10.1021/envhealth.4c00176
Environ. Health 2025, 3, 199−212

$MnCl_2{\cdot}4H_2O$ was added to drinking water at a Mn content of 200 mg/L for 5 weeks.

The *cGAS*$^{-/-}$ and *STING*$^{-/-}$ mice (C57BL/6J) were obtained from Dr. Zhengfan Jiang (Peking University). A sufficient number of offspring were obtained for subsequent experiments. The mice were randomly divided into *cGAS*$^{-/-}$ and *cGAS*$^{-/-}$+Mn, *STING*$^{-/-}$ and *STING*$^{-/-}$+Mn groups (10 mice per group). The feeding method, conditions, and dose and duration of Mn exposure were the same as those used for the WT mice. All the breeding and operation procedures for the mice were approved by the Institutional Review Committee of the School of Public Health, Lanzhou University (IRB23030501), and complied with the guidelines and regulations for the care and use of laboratory animals.

2.3. Collection of Animal Tissue Samples

At the end of the experiment, all the mice were anesthetized and sacrificed, and brain tissue was collected. Three brain tissues from each group of mice were fixed with 4% neutral paraformaldehyde. The remaining seven brain tissue samples were placed in cryopreservation tubes and stored at −80 °C.

2.4. RNA Sequencing (RNA-seq) Analysis

Total RNA was extracted with TRIzol Reagent (Life Technologies, California, USA). After measuring and assessing the concentration, purity and integrity of RNA, the qualified RNA was processed for library construction. Libraries with concentrations greater than 2 nmol/L determined by quantitative PCR (Q−PCR) were considered acceptable. The Illumina NovaSeq 6000 platform was used to sequence the libraries. DESeq2 was used for differential expression analysis. Genes with fold change (FC) ≥ 2 and adjusted false discovery rate (FDR) < 0.01 according to DESeq2 were considered differentially expressed. The clusterProfiler package was used for Gene Ontology (GO) enrichment analysis of the differentially expressed genes (DEGs). The statistical enrichment of DEGs in KEGG pathways were tested using the clusterProfiler software and KOBAS database. Biomarker Technologies performed the RNA-seq analysis.

Real-time PCR (RT−PCR) Master Mix (Sangon, Shanghai, China) was used to detect and quantify the expression of the target gene via the Biosystems StepTwo RT−PCR System (Applied Biosystems, USA). The following primer sequences were used for quantitative real-time PCR (qRT−PCR) to verify the RNA-seq results. *Apol9a*: Forward primer (10 μmol/L) 5′-AGGTCGGTGTGAACG-GATTTG-3′, Reverse primer (10 μmol/L) 5′-GAAGTCT-GCCTCTGTCTGCTATGG-3′; *Apol9b*: Forward primer (10 μmol/L) 5′-CCATAGCAGACAGAGGCAGACTTC-3′, Reverse primer (10 μmol/L) 5′-TGTGTAGTTTCTCAGCGTGGTCAG-3′; *CMPK2*: Forward primer (10 μmol/L) 5′-ACAGCCACCTAC-GCCATAGC-3′, Reverse primer (10 μmol/L) 5′-ACAGTCAGC-AGCAGGACCAAG-3′; *Irf5*: Forward primer (10 μmol/L) 5′-GACCACGCTGAGAAACTAC-3′, Reverse primer (10 μmol/L) 5′-GCTTCAACTTCATCCAAAACC-3′; *Isg15*: Forward primer (10 μmol/L) 5′-GAAGCAGATTGCCCAGAAG-3′, Reverse primer (10 μmol/L) 5′-GCGTCAGAAAGACCTCATAG-3′; *Ifi206*: Forward primer (10 μmol/L) 5′-GCAGTTACCAAAATTCCCCTC-3′, Reverse primer (10 μmol/L) 5′-GCTATGTCAAACACCTTCACTC-3′; *Ifit1*: Forward primer (10 μmol/L) 5′-GCACTGAACAACAAG-ACCC-3′, Reverse primer (10 μmol/L) 5′-GTCTTTCAGCCA-CTTTCTCC-3′; *β-actin*: Forward primer (10 μmol/L) 5′-GAT-GGTGGGAATGGGTCAGAAGG-3′, Reverse primer (10 μmol/L) 5′-TTGTAGAAGGTGTGGTGCCAGATC-3′.

2.5. Enzyme-Linked Immunosorbent Assay (ELISA)

The production of IFN-β in the culture supernatants of BV2 cells cultured with Mn^{2+} (100 μmol/L) for 6 h, was measured by ELISA according to the manufacturer's instructions (Elabscience, Wuhan, China). In brief, biotin, avidin, and other related reagents were added successively to form the immune complex. Finally, the color-developing substrate TMB (3,3,5,5-tetramethylbenzidine) was added, which appears blue under the catalysis of HRP and becomes yellow after the addition of the termination solution. The optical density (OD) was finally read at 450 nm with a microplate reader (Bio-Rad, USA), and the relative concentrations were calculated using standard curves.

2.6. Western Blot Analysis

The cells were lysed in RIPA buffer (AR0102, BOSTER, Wuhan, China) containing protease inhibitors (AR1178, BOSTER, Wuhan, China) and phosphatase inhibitors (K1015, Apexbio, USA). The protein content was determined, and the proteins were loaded onto 10% SDS−PAGE gels and transferred onto 0.45 μm polyvinylidene fluoride (PVDF) membranes (Millipore, Billerica, USA). After the membranes were blocked with 5% bovine serum albumin (BSA, A8020, Solarbio, Beijing, China), the membranes were probed with the following primary antibodies at 4 °C overnight: anti-LC3B (1:1,000; ab51520, Abcam, Cambridge, USA), anti-Beclin-1 (1:500; CQA1851, Cohesion Biosciences, Shanghai, China), anti-p62/SQSTM1 (1:1,000; ab155686, Abcam, Cambridge, USA), anticathepsin B (CTSB) (1:1,000; 12216−1-AP, Proteintech, USA), anti-cGAS (1:1,000; D3O8O, Cell Signaling Technology, USA), anti-ATG5 (1:1,000; ab108327, Abcam, USA), anti-Tau (1:1,000; ab32057, Abcam, Cambridge, USA), anti-STING (1:1,000; D2P2F, Cell Signaling Technology, USA), anti-β-actin (1:1,000; 13E5, Cell Signaling Technology, USA), anti-IRF3 (Interferon regulatory factor 3) (1:1,000; ab68481, Abcam, Cambridge, USA), anti-WIPI2 (1:1,000; bs-8767R, Bioss, Beijing, China) and anti-GAPDH (1:1,000; 52902, Signalway Antibody, USA), followed by incubation with a HRP-labeled secondary antibody (48139, Signalway Antibody, USA). The signals were visualized using a Western Bright ECL kit (S6009M, US EVERBRIGHT, Suzhou, China) and enhanced chemiluminescence (Bio-Rad, USA).

2.7. Immunofluorescence Assay

After fixation with 4% paraformaldehyde for 24 h, the brain tissue was cut into 4 μm thick sections using a microtome (RM2016, Leica, Germany). Then, deparaffinized, antigen retrieval and incubated with primary antibody (anti-p-Tau, Abcam, Cambridge, USA, phospho S404, ab92676, 1:300) at 4 °C overnight followed by blocking with 5% normal goat serum for 1 h. Afterward, the sections were washed three times with phosphate-buffered saline (PBS) and incubated with fluorescent secondary antibodies (1:200 dilution) at room temperature for 2 h. Fluorescence scanning microscope (P250 FLASH, Danjier Company, China) was used to observe the immunofluorescence (IF).

2.8. Statistical Analysis

Statistical analyses were performed with Prism 9 software (GraphPad Software, San Diego, CA, USA). All statistical analyses for data comparing two groups were performed with an unpaired Student's *t* test. One-way analysis of variance (ANOVA) with the Tukey−Kramer post hoc test for multiple comparisons was used for comparisons of more than two groups. The quantitative data are presented as the means ± standard deviations (SDs). $P < 0.05$ was considered statistically significant. All immunoblots are representative of results from at least three independent experiments.

3. RESULTS AND DISCUSSION

3.1. Mn Exposure Activates the cGAS−STING Pathway and Induces Type I IFN Production in Microglia

Innate immune responses is a common pathway for the initiation and progression of some NDDs,[49] and dysregulated innate and adaptive immune responses contribute to some NDDs.[50] The cGAS−STING pathway has been implicated in a number of NDDs.[51] Mn^{2+} has been found to be the second activator of the cGAS−STING pathway.[35,36] Therefore, we hypothesized that the potential neurotoxicity of Mn is related to abnormal activation of the cGAS−STING pathway. Autopsy reports from Mn-exposed patients show abnormal activation of astrocytes and microglia.[52] Microglia are brain-resident cells and are key components of the brain's innate immune

https://doi.org/10.1021/envhealth.4c00176
Environ. Health 2025, 3, 199−212

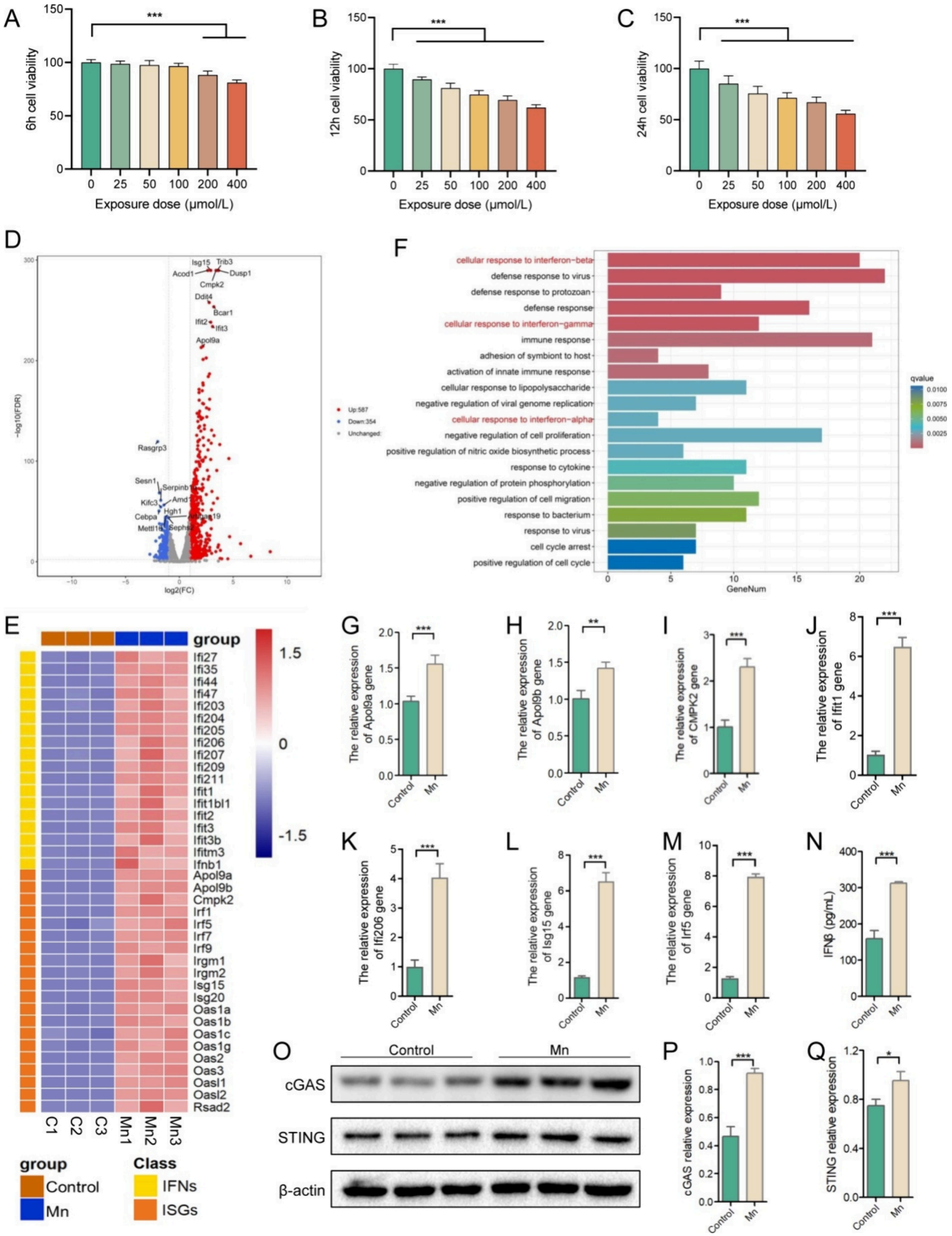

Figure 1. Mn exposure activates the cGAS−STING−IFN-I pathway in microglia. (**A**-**C**), Activity of BV2 cells treated with different doses of Mn for 6, 12, and 24 h. (**D**), Volcano plot of RNA-seq data from BV2 cells untreated or treated with $MnCl_2$ (100 μmol/L) for 6 h. Red and blue dots

https://doi.org/10.1021/envhealth.4c00176
Environ. Health 2025, 3, 199−212

Figure 1. continued

represent genes with a log2 FC > 2 and < − 2, respectively. (**E**), Heatmap of the RNA-seq date. BV2 cells were untreated or treated with $MnCl_2$ (100 μmol/L) for 6 h. (**F**), Gene set enrichment analysis showing hallmark pathways associated with the differentially expressed genes upregulated in the BV2 cell samples treated with $MnCl_2$ for 6 h compared with the control samples. (**G**-**M**), RT−qPCR analysis of the expression of the *Apol9a*, *Apol9b*, *CMPK2*, *Ifit1*, *Ifi206*, *Isg15* and *Irf5* genes in BV2 cells untreated or treated with $MnCl_2$ (100 μmol/L) for 6 h. (**N**), IFN-β changes in BV2 cell (10^6/mL) culture supernatants were detected by ELISA. (**O**-**Q**), BV2 cells were treated with $MnCl_2$ for 6 h. Western blot analysis was used to analyze cGAS and STING. Three independent experiments were performed three times. The error bars represent the SDs; the CCK-8 data were analyzed by one-way ANOVA with the Tukey−Kramer post hoc test for multiple comparisons, and the other data were analyzed by an unpaired *t* test. *P < 0.05; **P < 0.01; ***P < 0.001.

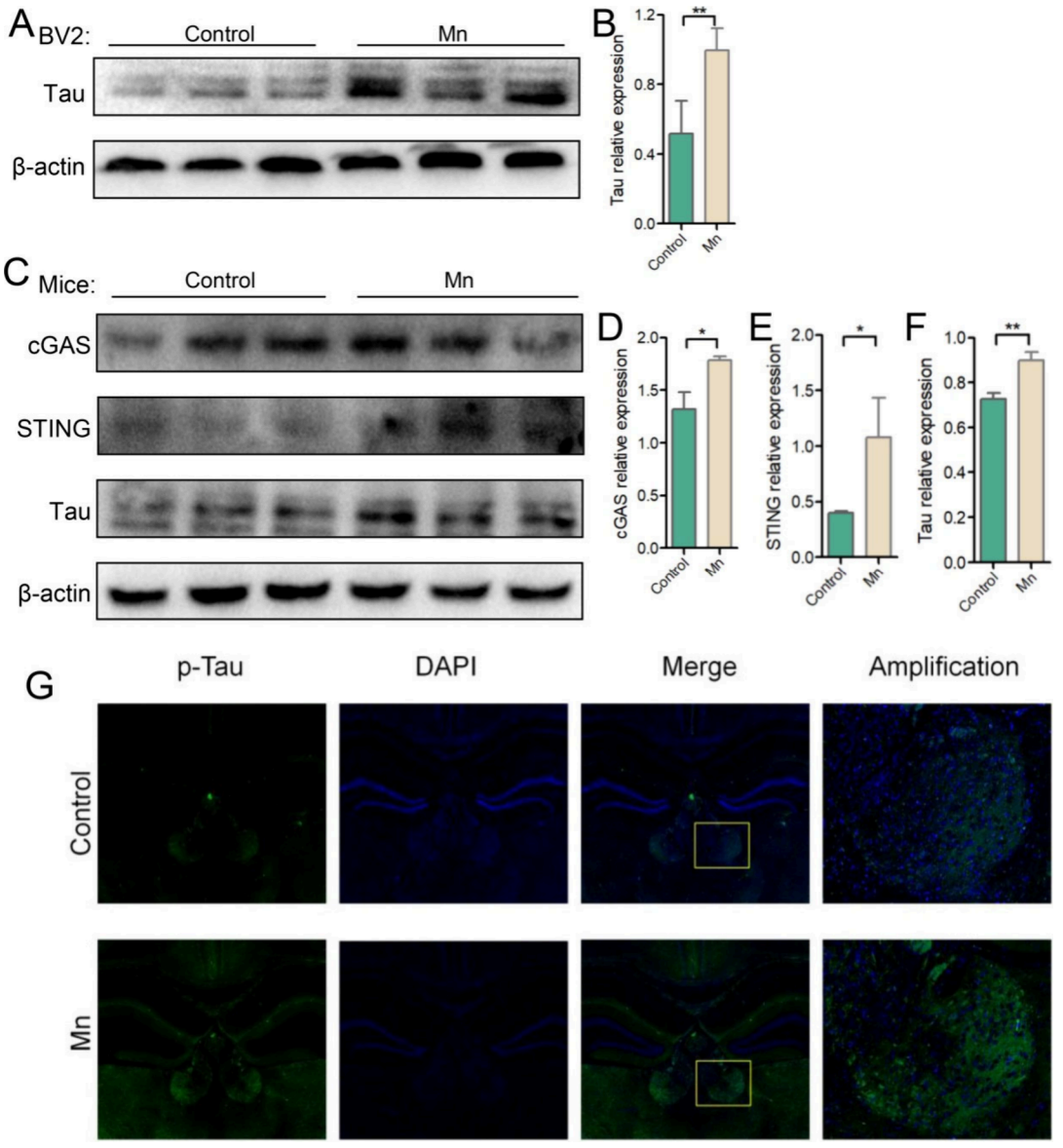

Figure 2. Mn exposure activates the cGAS−STING pathway while inducing Tau aggregation. (**A**, **B**), BV2 cells were treated with $MnCl_2$ for 6 h. Tau expression was analyzed by Western blotting. (**C**-**F**), Western blot analysis of cGAS, STING and Tau expression in the brains of Mn-exposed mice. (**G**), p-Tau expression in the brain was detected by immunofluorescence. Three independent experiments were performed three times. The error bars represent the SDs; the data were analyzed by an unpaired *t* test. *P < 0.05; **P < 0.01; ***P < 0.001.

response.[53] Microglia are involved in Tau-mediated pathobiology, and microglial activation is a prominent pathological feature of tauopathies.[49] Microglia serve as the leading driving force of neurodegeneration and Tau pathogenesis in tauopathy mouse models.[54] The cGAS−STING−IFN response occurs mainly in the microglia of the brain during AD and aging.[33] It has been reported that aberrant microglial cGAS−STING−IFN activation may drive neuronal MEF2C deficiency and that MEF2C is an AD risk gene that compromises cognitive resilience.[55] Thus, BV2 microglia were selected for *in vitro* experiments in this study.

First, the CCK-8 method was used to measure the effects of Mn exposure at different times and concentrations on the proliferative activity of BV2 cells. According to the results of

https://doi.org/10.1021/envhealth.4c00176
Environ. Health 2025, 3, 199−212

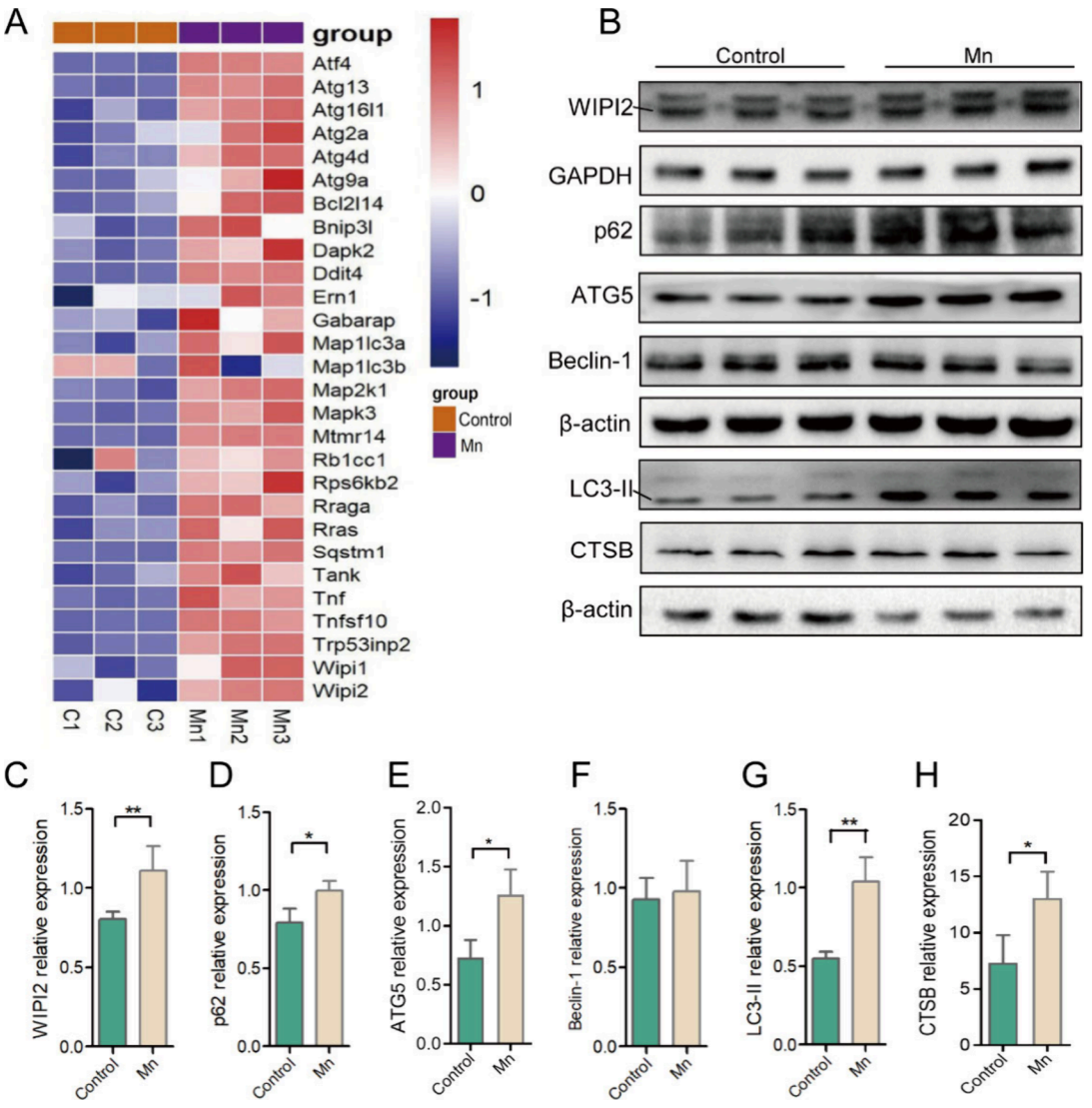

Figure 3. Mn exposure causes autophagy−lysosomal pathway dysfunction. (**A**), Heatmap summary of autophagy-related genes that are most highly expressed in BV2 cells stimulated with Mn. (**B**-**H**), BV2 cells were treated with $MnCl_2$ for 6 h. The protein levels of WIPI2, p62, ATG5, Beclin-1, LC3-II and CTSB were analyzed by Western blotting and statistically analyzed. Three independent experiments were performed three times. The error bars represent the SDs; the data were analyzed by an unpaired *t* test. *$P < 0.05$; **$P < 0.01$; ***$P < 0.001$.

the CCK-8 assay, 100 μmol/L $MnCl_2$ for 6 h was selected for subsequent experiments (Figure 1A-C). The volcano plot and heatmap of the DEGs identified via RNA-seq analysis of Mn-treated BV2 microglia revealed that Mn exposure induced robust production of both IFNs and IFN-stimulated genes (ISGs), including *Ifit2*, *Ifi27*, *Isg15*, *Oas1a*, *Dusp1*, and *Irf7*, among others (Figure 1D,E). KEGG analysis showed that the DEGs were related mainly to IFN pathways (Figure 1F). In mammals, the most prominent function of the cGAS−STING pathway is the production of IFN-I.[56] We confirmed the results of the DEGs (*Apol9a*, *Apol9b*, *CMPK2*, *Ifit1*, *Ifi206*, *Isg15*, and *Irf5*) by qRT−PCR (Figure 1G-M), and the production of IFN-β was also verified by ELISA (Figure 1N). Compared with the control, Mn exposure significantly increased the protein levels of cGAS and STING in BV2 microglia, as shown by immunoblotting (Figure 1O-Q). Our results demonstrate that Mn exposure activates the cGAS−STING pathway and induces type IFN-I production in microglia.

3.2. The cGAS−STING Pathway Activated by Mn Exposure Induces Tauopathy in Microglia and in Mice

Activated ISGs and IFN-I-expressing microglia are significantly correlated with AD severity.[57] The potential neurotoxicity of Mn is related to the neurodevelopment and developmental risk of AD and PD.[19] Tau pathology accumulation is more closely associated with synaptic loss, neuronal apoptosis, neurodegeneration, and cognitive decline than amyloid deposition.[58,59] Tau oligomers with seed toxicity and altered dissolution properties are considered to be the main toxic form of NDDs.[60] To test the hypothesis that cGAS−STING pathway activation drives tauopathy, Tau expression was assessed. Compared with the control, Mn exposure significantly increased the level of Tau expression in BV2 cells, as shown by immunoblotting (Figure 2A,B). We then constructed a mouse model to explore the effect of Mn exposure on Tau aggregation *in vivo*. Mn exposure increased the levels of Tau (p-Tau) in the whole brains of the mice while activating the cGAS−STING pathway, as shown by immunoblotting (Figure 2C−F) and immunofluorescence (Figure 2G). *In vitro*

https://doi.org/10.1021/envhealth.4c00176
Environ. Health 2025, 3, 199−212

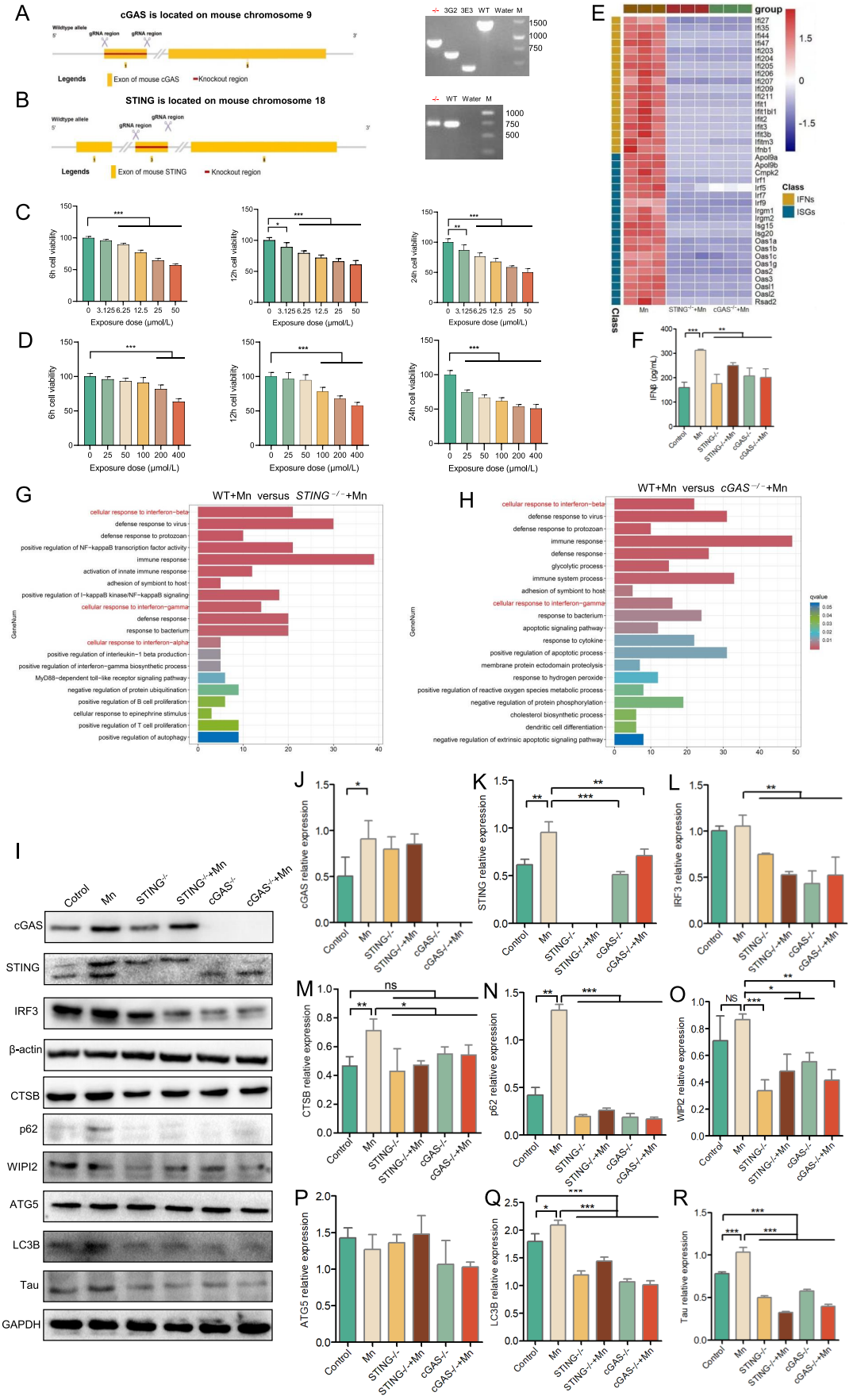

Figure 4. Inhibition of the cGAS−STING pathway restores the function of the autophagy−lysosomal pathway and promotes Tau degradation. (**A**), Schematic strategy for the generation of *cGAS* knockout BV2 cells and representative agarose gel electrophoresis images for the genotyping of

https://doi.org/10.1021/envhealth.4c00176
Environ. Health 2025, 3, 199−212

Figure 4. continued

cGAS$^{-/-}$ cells. (**B**), Schematic strategy for the generation of *STING* knockout BV2 cells and representative images of agarose gel electrophoresis results for the genotyping of *STING*$^{-/-}$ cells. (**C**), Activity of BV2$^{cGAS-/-}$ cells treated with different doses of $MnCl_2$ for 6, 12, and 24 h. (**D**), Activity of BV2$^{STING-/-}$ cells treated with different doses of $MnCl_2$ for 6, 12, and 24 h. (**E**), Heatmap of the RNA-seq date. (**F**), IFN-β changes in BV2 cell (10^6/mL) culture supernatants were detected by ELISA. (**G-H**), GO analysis showing the downregulated biological processes in BV2$^{STING-/-}$ and BV2$^{cGAS-/-}$ cells compared with those in WT cells after $MnCl_2$ treatment. (**I-R**), The protein levels of cGAS, STING, IRF3, CTSB, p62, WIPI2, ATG5, LC3B and Tau were analyzed by Western blotting and statistically analyzed in BV2, BV2$^{cGAS-/-}$ and BV2$^{STING-/-}$ cells after Mn stimulation. Three independent experiments were performed three times. The error bars represent the SDs; the data were analyzed by one-way ANOVA with the Tukey−Kramer post hoc test for multiple comparisons. *P < 0.05; **P < 0.01; ***P < 0.001; NS, not significant.

and *in vivo* experiments demonstrated that Mn exposure induced tauopathy while activating the cGAS−STING pathway. The inhibition of Tau aggregation may be a strategy for the treatment of NDDs induced by Mn exposure.

3.3. Mn Exposure Impairs the Dysfunction of the Autophagy−Lysosomal Pathway

Recently, the induction of autophagy has been shown to be is a primordial function of the cGAS−STING pathway.[61] Autophagy dysfunction is involved in the pathology of NDDs.[21,62] The autophagy−lysosomal pathway plays a critical role in the maintenance of cellular homeostasis by removing misfolded proteins and damaged organelles.[63] Impairment of the function of the autophagy−lysosomal pathway is associated with neuronal cell death[64] and major NDDs.[65−67] Disruption of multiple steps of autophagy and dysfunctional autophagosome clearance may occur in neurons during AD pathogenesis.[65,68] Microglial autophagy plays a protective role in regulating amyloid plaque homeostasis and restricting senescence, and autophagy deficiency promotes senescence-associated microglia.[69] Loss of microglial autophagy exacerbates Tau spread and pathology in a tauopathy model.[70] Thus, we explored the effect of Mn exposure on the autophagy−lysosomal pathway. Our RNA-seq results revealed that Mn exposure increased the expression of autophagy-related genes (*Wipi1*, *Wipi2*, *Atg13*, *Atg4d*, and *Tnf*, among others; Figure 3A). To study Mn exposure induced dysfunction of the autophagy−lysosomal pathway, the key proteins WIPI2, p62/SQSTM1, ATG5, Beclin-1, CTSB and LC3B were detected in BV2 cells. Mn exposure stimulated the conversion of LC3 into a lipidated form (LC3-II) (Figure 3B,G) and promoted WIPI2 expression (Figure 3B,C). LC3 lipid is an autophagosomal surface protein marker and is a key step in autophagosome biogenesis.[61,71] Our results were consistent with the finding that the cGAS−STING pathway induces LC3 lipidation.[61] However, at the same time, we also observed the accumulation of p62 (Figure 3B,D) and CTSB (Figure 3B,H) in Mn-exposed BV2 cells. The p62 protein is a chaperone protein involved in autophagy degradation.[72] It is also a significant component in the autophagy−lysosomal pathway, which has also been shown to deliver ubiquitinated proteins (such as Tau) to the proteasome for degradation.[73] Recent evidence has shown that p62 is highly associated with the protein-degrading system and the progression of vulnerability in Alzheimer's.[74] In this study, the increased accumulation of p62 in cells reflects that autophagosomes cannot be degraded by lysosomes after Mn exposure. CTSB is an indicator of lysosomal function, and lysosomal dysfunction leads to CTSB accumulation in the cell.[75] Lysosomal function can be assessed by CTSB expression.[76] Increased CTSB expression and activity are important triggers for the pathological development of numerous diseases.[33] In the present study, increased CTSB expression suggested that Mn exposure causes abnormal lysosomal function in BV2 microglia. Taken together, the significantly elevated LC3-II, p62, WIPI2, ATG5 and CTSB levels indicate impaired function of the autophagy−lysosomal pathway induced by Mn exposure. These results are similar to reports that Mn exposure induces autophagy−lysosomal pathway dysfunction by inducing a decrease in the nuclear localization of transcription factor EB (TFEB) and by increasing CTSB levels.[76,77] These findings suggest that impairs the autophagy−lysosomal pathway function might be responsible for the accumulation of Tau (p-Tau) in Mn exposure.

3.4. Inhibiting the cGAS−STING Pathway Rescues the Autophagy−Lysosomal Pathway Dysfunction and Tauopathy in Microglia Induced by Mn Exposure

Given the key role of the cGAS−STING pathway in autophagy and NDDs, we hypothesized that the cGAS−STING pathway might mediate the function of the autophagy−lysosomal pathway and thereby regulate tauopathy induced by Mn exposure. Therefore, global *cGAS*- and *STING*-knockout (*cGAS*$^{-/-}$ and *STING*$^{-/-}$) BV2 microglia were generated via CRISPR/Cas9. The *cGAS* gene is located on mouse chromosome 9, and a total of 5 exons have been identified, with the ATG start codon in exon 1 and the TGA stop codon in exon 5. Exon 1 was selected as the target site (Figure 4A). The *STING* gene is located on mouse chromosome 18, and a total of 8 exons have been identified, with the ATG start codon in exon 3 and the TGA stop codon in exon 8. Exon 3 was selected as the target site (Figure 4B). *cGAS*$^{-/-}$ and *STING*$^{-/-}$ microglia were further confirmed by PCR (Figure 4A,B) and Western blot analysis (Figure 4I), and the results showed that the cGAS and STING proteins were completely abolished in the homozygous targeted allele. In accordance with the results of CCK-8 assay, 3.125 μmol/L and 100 μmol/L $MnCl_2$ were added to BV2$^{cGAS-/-}$ and BV2$^{STING-/-}$ cells, respectively, for 6 h for subsequent experiments (Figure 4C,D). Inhibition of STING activation has been reported to prevent the deleterious effects of IFN responses in PD and amyotrophic lateral sclerosis (ALS).[32,78] RNA-seq and ELISA analyses of BV2$^{STING-/-}$ and BV2$^{cGAS-/-}$ cells revealed that blocking the cGAS−STING pathway completely inhibited the production of both IFNs and ISGs induced by Mn exposure (Figure 4E,F), suggesting that the induction of IFN-I production by $MnCl_2$ depends on the cGAS−STING pathway. GO analysis revealed that the downregulated biological processes in BV2$^{STING-/-}$ and BV2$^{cGAS-/-}$ cells were related mainly to the IFN pathway compared with those in WT cells after $MnCl_2$ treatment (Figure 4G,H).

To determine whether blocking the cGAS−STING pathway can rescue impaired autophagy−lysosomal pathway function, the expression of the autophagy−lysosomal pathway-related proteins CTSB, p62, LC3-II, ATG5 and WIPI2 in BV2$^{STING-/-}$ and BV2$^{cGAS-/-}$ cells was detected after Mn exposure. The

https://doi.org/10.1021/envhealth.4c00176
Environ. Health 2025, 3, 199−212

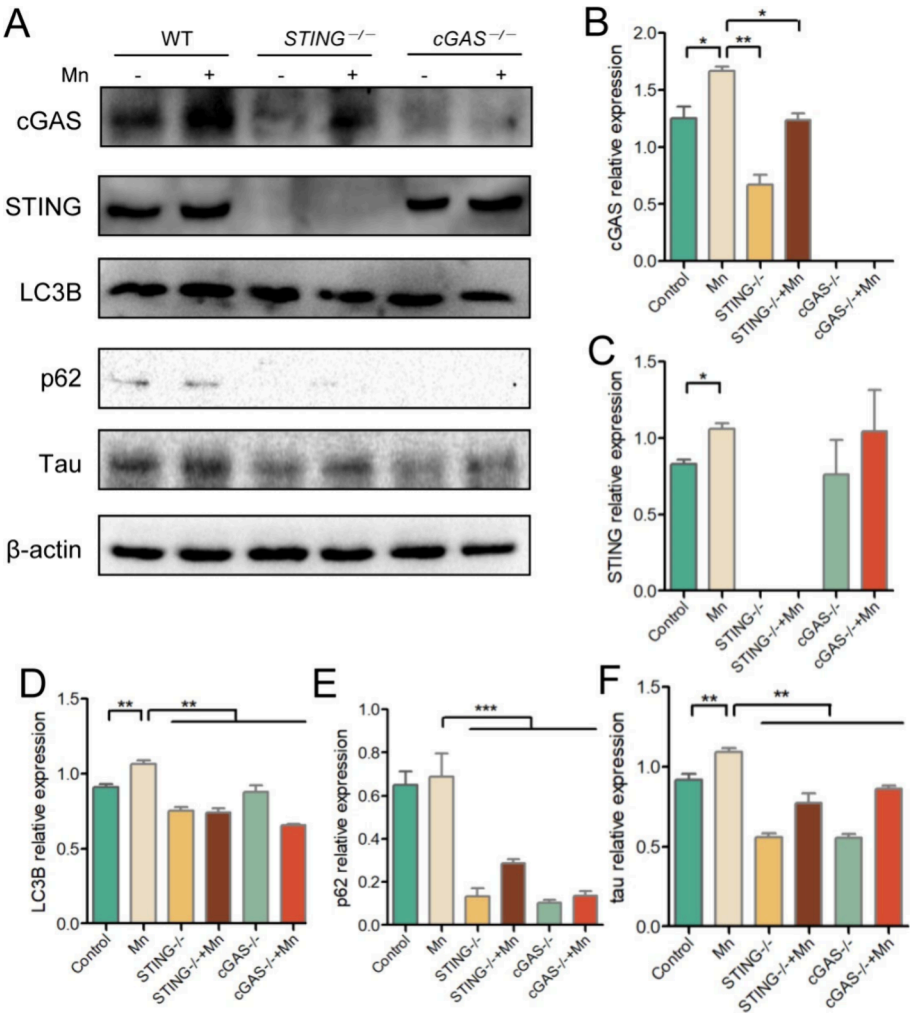

Figure 5. Mn exposure activates the cGAS−STING pathway to mediate Tau aggregation and autophagy−lysosomal pathway dysfunction. (**A**-**F**), The protein levels of cGAS, STING, LC3B, p62 and Tau in the brains of WT, *cGAS*$^{-/-}$ and *STING*$^{-/-}$ mice were analyzed by Western blotting and statistically analyzed after Mn exposure. Three independent experiments were performed three times. The error bars represent the SDs; the data were analyzed by one-way ANOVA with the Tukey−Kramer post hoc test for multiple comparisons. *P < 0.05; **P < 0.01; ***P < 0.001.

results showed that blocking the cGAS−STING pathway rescued the dysfunction of the autophagy−lysosomal pathway (Figure 4I-Q), as indicated by decreased expression of WIPI2, LC3B, CTSB and p62. Moreover, when the cGAS−STING pathway was inhibited, the increased expression of Tau induced by Mn exposure was significantly decreased (Figure 4I,R). Impaired autophagy−lysosomal pathway function leads to a decreased clearance of Tau.[79,80] As expected, the autophagy−lysosomal pathway function was enhanced after *cGAS* and *STING* knockout. These results demonstrated that inhibition of the cGAS−STING pathway protects against microglial autophagy−lysosomal pathway dysfunction and tauopathy induced by Mn exposure.

3.5. Inactivation of the cGAS−STING Pathway Restores the Function of the Autophagy−Lysosomal Pathway and Protects Against Tauopathy Induced by Mn Exposure in Mice

We further determined the effects of cGAS−STING pathway inactivation on the function of the autophagy−lysosomal pathway and tauopathy *in vivo* using *cGAS*- and *STING*-knockout (*cGAS*$^{-/-}$ and *STING*$^{-/-}$) mice. In Mn-treated mice, cGAS, STING and Tau expression was significantly greater than that in control mice (Figure 5A-C,F). The results showed that Mn induced tauopathy while activating the cGAS−STING pathway, which is in agreement with the *in vitro* results. Surprisingly, the increases in the expression of LC3B, p62 and Tau induced by Mn exposure were significantly decreased after cGAS−STING pathway inhibition (Figure 5A,D-F). The results indicate that inactivation of the cGAS−STING pathway not only alleviated Mn-induced the autophagy−lysosomal pathway dysfunction but also markedly decreased Tau expression in brains of the mice. Several studies have demonstrated that STING activation is indispensable for autophagy induction[81] and that STING degradation occurs through the autophagy−lysosomal pathway.[82] These findings indicate that the neurotoxicity of tauopathy and autophagy−lysosomal pathway dysfunction induced by Mn exposure are regulated through the cGAS−STING pathway-dependent responses, which are reduced by cGAS−STING pathway inhibition. In summary, we found that *cGAS* and *STING* deficiency markedly attenuated tauopathy induced by Mn exposure *in vitro* and *in vivo*, likely by ameliorating the function of the autophagy−lysosomal pathway, which is an exciting new finding. Therefore, the cGAS−STING pathway inhibition could be a promising strategy for activating the autophagy−lysosomal pathway and potentially alleviating tauopathy.

https://doi.org/10.1021/envhealth.4c00176
Environ. Health 2025, 3, 199−212

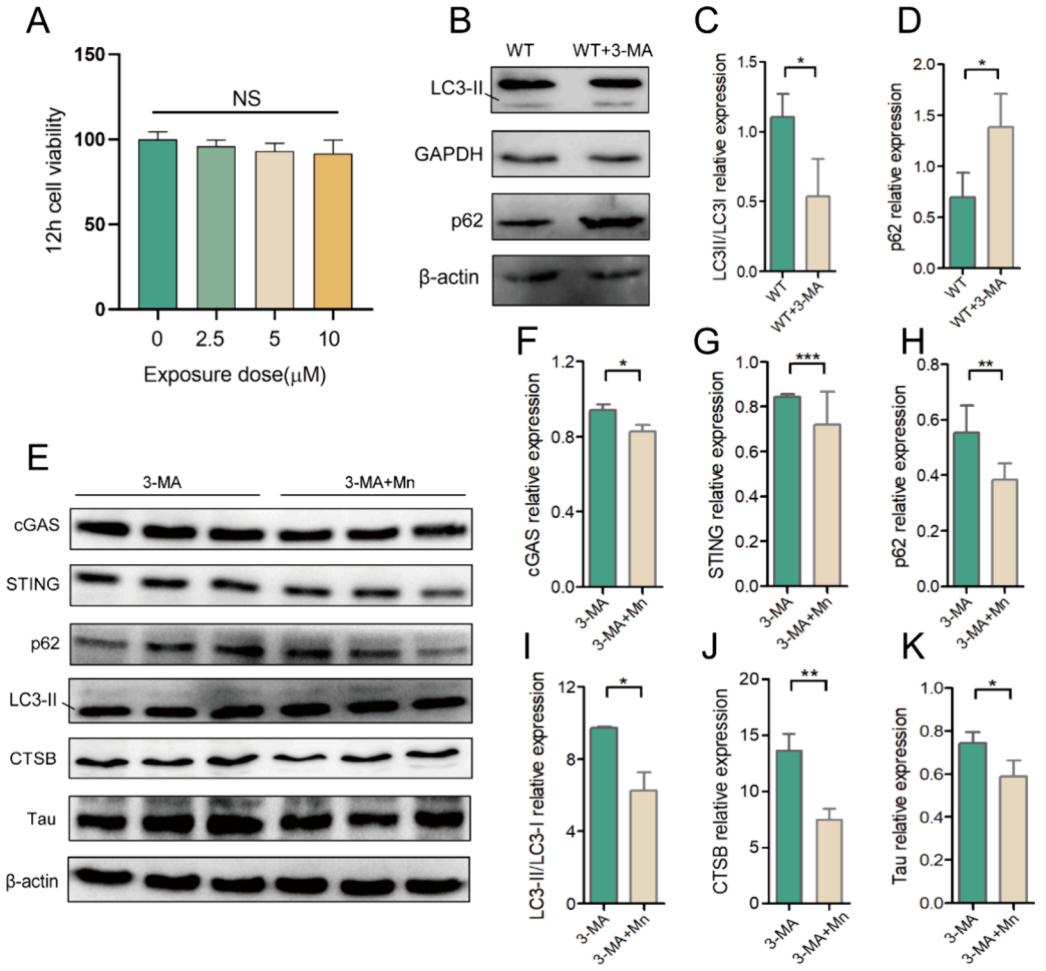

Figure 6. 3-MA ameliorates tauopathy induced by Mn exposure by inactivating the cGAS−STING pathway through the autophagy−lysosomal pathway. (**A**), Activity of BV2 cells treated with different doses of 3-MA for 12 h, as detected by the CCK-8 method. (**B-D**), Western blot analysis of autophagy blockade. (**E-K**), The protein levels of cGAS, STING, p62, LC3-II, CTSB and Tau in BV2 microglia were analyzed by Western blotting and statistically analyzed after Mn exposure. Three independent experiments were performed three times. The error bars represent the SDs; the CCK-8 data were analyzed by one-way ANOVA with the Tukey−Kramer post hoc test for multiple comparisons, and the other data were analyzed by an unpaired *t* test. $^{*}P < 0.05$; $^{**}P < 0.01$; $^{***}P < 0.001$; NS, not significant.

3.6. 3-MA Ameliorates Tauopathy by Inactivating the cGAS−STING Pathway through the Autophagy−Lysosomal Pathway

To further validate the important role of autophagy−lysosomal function in Mn exposure, we selectively inactivated autophagy in microglia with 3-MA. As previously described, SH-SY5Y cells were treated with 10 μmol/L 3-MA for 12 h before Mn exposure.[83] CCK-8 experiments revealed that treatment of BV2 cells with 2.5, 5, or 10 μmol/L 3-MA for 12 h did not affect cell proliferation activity (Figure 6A); therefore, we selected 10 μmol/L 3-MA for 12 h to inactivate autophagy before Mn exposure. Blocking of autophagy in BV2 cells was confirmed by Western blotting (Figure 6B-D). The expression of cGAS and STING in BV2 cells increased after Mn treatment, as shown in Figure 1, while Western blot analysis revealed that autophagy blocked by 3-MA inhibited this effect (Figure 6E-G). Mn exposure impaired the function of the autophagy−lysosomal pathway, but the effect was reversed by the addition of 3-MA to BV2 cells, as indicated by the reduced expression of LC3-II/LC3-I, CTSB and p62 (Figure 6E,H-J). In addition, the tauopathy induced by Mn exposure was reversed by treatment with 3-MA (Figure 6E,K). We further demonstrated that pretreatment with autophagy inhibitor (3-MA) partially prevented the accumulation of the lysosomal marker CTSB by inhibiting the cGAS−STING pathway activated by Mn exposure, which in turn restored the impaired autophagy−lysosomal pathway function to clear Tau accumulation. Dysfunctional lysosomal storage may occur after upregulation of neuronal autophagy. Our findings are similar to the report that an initial upregulation of autophagy and dysfunctional lysosomal storage occur during acute ischemia, which can be prevented by inhibiting autophagy with 3-MA.[84] Therefore, pharmacological approaches aimed at inhibiting the cGAS−STING−autophagy−lysosomal axis to attenuate Mn-induced tauopathy may confer neuroprotection. In addition, whether typical AD and PD also have similar pathogeneses should be investigated in the future.

4. CONCLUSIONS

Mn exposure induces tauopathy by activating the cGAS−STING pathway. Mn exposure also impairs the function of the autophagy−lysosomal pathway and blocks the degradation of Tau through this pathway. Ultimately, Mn exposure induces autophagy−lysosomal pathway dysfunction by activating the cGAS−STING pathway, leading to Tau accumulation in the brain and triggering potential neurotoxicity (Figure 7).

https://doi.org/10.1021/envhealth.4c00176
Environ. Health 2025, 3, 199−212

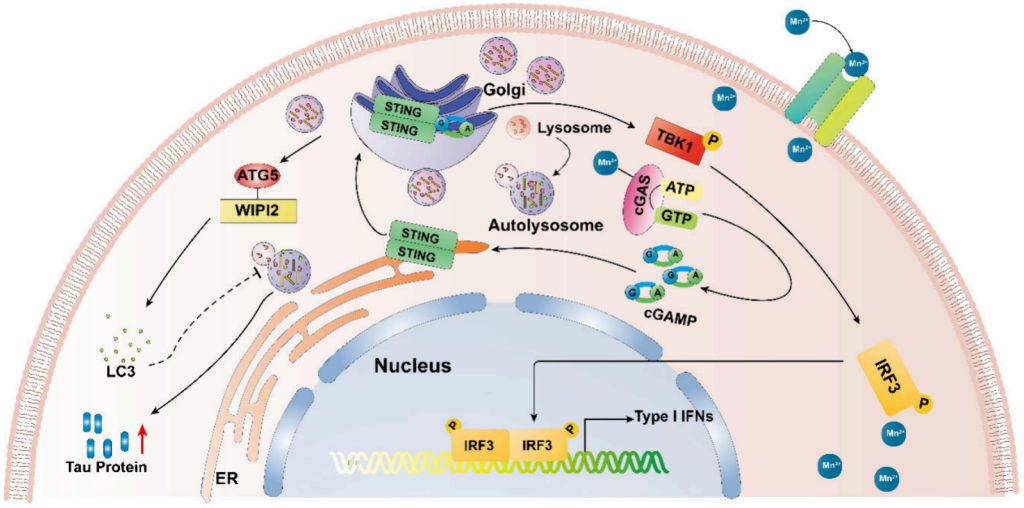

Figure 7. Mn exposure induces tauopathy by impairing the function of the autophagy−lysosomal pathway through activation of the cGAS−STING pathway.

Therefore, the cGAS−STING−autophagy−lysosomal axis plays a crucial role in Mn exposure-induced tauopathy, which highlight the underlying mechanism of Mn neurotoxicity. These findings provide drug targets for future research on the prevention and control of the neurotoxicity of Mn, an environmental pollutant, and provide scientific insights into the mechanism of environmental toxicants from the perspective of innate immune system disorders.

AUTHOR INFORMATION

Corresponding Author

Hui Wang − *Department of Toxicology, School of Public Health, Lanzhou University, Gansu 730000, China;* orcid.org/0000-0002-4136-0999; Email: huiwang@lzu.edu.cn

Authors

Xin Zhang − *Department of Toxicology, School of Public Health, Lanzhou University, Gansu 730000, China*

Jingjing Liu − *Department of Toxicology, School of Public Health, Lanzhou University, Gansu 730000, China*

Shiyin Zhong − *Department of Toxicology, School of Public Health, Lanzhou University, Gansu 730000, China*

Zhimin Zhang − *Department of Toxicology, School of Public Health, Lanzhou University, Gansu 730000, China*

Qiongli Zhou − *Department of Toxicology, School of Public Health, Lanzhou University, Gansu 730000, China*

Jirui Yang − *Department of Toxicology, School of Public Health, Lanzhou University, Gansu 730000, China*

Xuhong Chang − *Department of Toxicology, School of Public Health, Lanzhou University, Gansu 730000, China*

Complete contact information is available at: https://pubs.acs.org/10.1021/envhealth.4c00176

Notes

The authors declare no competing financial interest.

ACKNOWLEDGMENTS

This work was supported by the Medical Innovation and Development Project of Lanzhou University (No. lzuyxcx-2022-196), Startup Fund for the Construction of the Double First-Class Project of Lanzhou University (No. 561121203), Lanzhou Youth Science and Technology Talent Innovation Project (2023-QN-60), and National Natural Science Foundation of China (No. 31802256). The authors would like to extend the gratitude to Dr. Zhengfan Jiang at Peking University for providing *cGAS*$^{-/-}$ and *STING*$^{-/-}$ mice. Thanks to Biomarker Technologies for the RNA-seq analysis.

ABBREVIATIONS

AD, Alzheimer's disease; ANOVA, analysis of variance; ATG, autophagy-related gene; Aβ, amyloid β-protein; CCK-8, cell counting kit-8; cGAS, cyclic GMP-AMP synthase; CTSB, cathepsin B; DEGs, differentially expressed genes; dsDNA, double-stranded DNA; FC, fold change; FDR, false discovery rate; GO, gene ontology; IFN, interferon; IRF3, interferon regulatory factor 3; ISGs, interferon stimulated genes; LC3, microtubule-associated protein light chain 3; Mn, manganese; NDDs, neurodegenerative diseases; PCR, polymerase chain reaction; PD, Parkinson's disease; RNA-seq, RNA sequencing; ROS, reactive oxygen species; RT−PCR, real-time polymerase chain reaction; SD, standard deviation; STING, stimulator of interferon gene; WT, wild-type; 3-MA, 3-methyladenine

REFERENCES

(1) Wilson, D. M., 3rd; Cookson, M. R.; Van Den Bosch, L.; Zetterberg, H.; Holtzman, D. M.; Dewachter, I. Hallmarks of neurodegenerative diseases. *Cell* **2023**, *186* (4), 693−714.

(2) Dugger, B. N.; Dickson, D. W. Pathology of Neurodegenerative Diseases. *Cold Spring Harb. Perspect. Biol.* **2017**, *9* (7), a028035.

(3) Wang, H.; Yang, F.; Zhang, S.; Xin, R.; Sun, Y. Genetic and environmental factors in Alzheimer's and Parkinson's diseases and promising therapeutic intervention via fecal microbiota transplantation. *NPJ. Parkinsons. Dis.* **2021**, *7* (1), 70.

(4) Bakulski, K. M.; Seo, Y. A.; Hickman, R. C.; Brandt, D.; Vadari, H. S.; Hu, H.; Park, S. K. Heavy Metals Exposure and Alzheimer's Disease and Related Dementias. *J. Alzheimers Dis.* **2020**, *76* (4), 1215−1242.

(5) Vellingiri, B.; Suriyanarayanan, A.; Selvaraj, P.; Abraham, K. S.; Pasha, M. Y.; Winster, H.; et al. Role of heavy metals (copper (Cu), arsenic (As), cadmium (Cd), iron (Fe) and lithium (Li)) induced neurotoxicity. *Chemosphere* **2022**, *301*, 134625.

(6) Pinsino, A., Matranga, V., Roccheri, M. C. Manganese: a new emerging contaminant in the environment. In: Srivastava, J. (Ed.),

Environmental Contamination. In Tech Open Access Publisher, Rijeka, Croatia, 2012; pp 17−36.
(7) Favas, P. J. C.; Sarkar, S. K.; Rakshit, D.; Venkatachalam, P.; Prasad, M. N. V. Acid mine drainages from abandoned mines: hydrogeochemistry, environmental impact, resource recovery, and prevention of pollution. In: Prasad, M. N. V.; Shih, K. (Eds.), *Environmental Materials and Waste, Resource Recovery and Pollution Prevention*. Elsevier, Academic Press, 2016; pp 413e462.
(8) Zhao, T.; Lv, W. H.; Hogstrand, C.; Zhang, D. G.; Xu, Y. C.; Xu, Y. H.; Luo, Z. Sirt3-Sod2-mROS-mediated manganese triggered hepatic mitochondrial dysfunction and lipotoxicity in a freshwater teleost. *Environ. Sci. Technol.* **2022**, *56* (12), 8020−8033.
(9) Huat, T. J.; Camats-Perna, J.; Newcombe, E. A.; Valmas, N.; Kitazawa, M.; Medeiros, R. Metal toxicity links to alzheimer's disease and neuroinflammation. *J. Mol. Biol.* **2019**, *431* (9), 1843−1868.
(10) Fernández-Olmo, I.; Mantecón, P.; Markiv, B.; Ruiz-Azcona, L.; Santibáñez, M. A Review on the Environmental Exposure to Airborne Manganese, Biomonitoring, and Neurological/Neuropsychological Outcomes. *Rev. Environ. Contam. Toxicol.* **2020**, *254*, 85−130.
(11) Peres, T. V.; Schettinger, M. R.; Chen, P.; Carvalho, F.; Avila, D. S.; Bowman, A. B.; Aschner, M. ″Manganese-induced neurotoxicity: a review of its behavioral consequences and neuroprotective strategies″. *BMC Pharmacol. Toxicol.* **2016**, *17* (1), 57.
(12) Dayan, R.; Arkadir, D. Manganese Accumulation in the Brain. *N. Engl. J. Med.* **2023**, *389* (14), 1320.
(13) Budinger, D.; Barral, S.; Soo, A. K. S.; Kurian, M. A. The role of manganese dysregulation in neurological disease: emerging evidence. *Lancet Neurol.* **2021**, *20* (11), 956−968.
(14) Iyare, P. U. The effects of manganese exposure from drinking water on school-age children: a systematic review. *Neurotoxicology* **2019**, *73*, 1−7.
(15) Racette, B. A.; Nelson, G.; Dlamini, W. W.; Hershey, T.; Prathibha, P.; Turner, J. R.; et al. Environmental manganese exposure and cognitive control in a South African population. *Neurotoxicology* **2022**, *89*, 31−40.
(16) Racette, B. A.; Nelson, G.; Dlamini, W. W.; Hershey, T.; Prathibha, P.; Turner, J. R.; et al. Depression and anxiety in a manganese-exposed community. *Neurotoxicology* **2021**, *85*, 222−233.
(17) DeSimone, L. A.; McMahon, P. B.; Rosen, M. R. The quality of our Nation's waters: Water quality in principal aquifers of the United States, 1991−2010, *Circular*. Reston, VA, 2015; p 161.
(18) Ramachandran, M.; Schwabe, K. A.; Ying, S. C. Shallow Groundwater Manganese Merits Deeper Consideration. *Environ. Sci. Technol.* **2021**, *55* (6), 3465−3466.
(19) Balachandran, R. C.; Mukhopadhyay, S.; McBride, D.; Veevers, J.; Harrison, F. E.; Aschner, M.; Haynes, E. N.; Bowman, A. B. Brain manganese and the balance between essential roles and neurotoxicity. *J. Biol. Chem.* **2020**, *295* (19), 6312−6329.
(20) Schullehner, J.; Thygesen, M.; Kristiansen, S. M.; Hansen, B.; Pedersen, C. B.; Dalsgaard, S. Exposure to Manganese in Drinking Water during Childhood and Association with Attention-Deficit Hyperactivity Disorder: A Nationwide Cohort Study. *Environ. Health Perspect.* **2020**, *128* (9), 097004.
(21) Zhang, X.; Liu, J.; Wang, H. The cGAS-STING-autophagy pathway: Novel perspectives in neurotoxicity induced by manganese exposure. *Environ. Pollut.* **2022**, *315*, 120412.
(22) Lucchini, R. G.; Aschner, M.; Landrigan, P. J.; Cranmer, J. M. Neurotoxicity of manganese: Indications for future research and public health intervention from the Manganese 2016 conference. *Neurotoxicology* **2018**, *64*, 1−4.
(23) Huang, Q.; Wan, J.; Nan, W.; Li, S.; He, B.; Peng, Z. Association between manganese exposure in heavy metals mixtures and the prevalence of sarcopenia in US adults from NHANES 2011−2018. *J. Hazard. Mater.* **2024**, *464*, 133005.
(24) Karyakina, N. A.; Shilnikova, N.; Farhat, N.; Ramoju, S.; Cline, B.; Momoli, F.; et al. Biomarkers for occupational manganese exposure. *Crit. Rev. Toxicol.* **2022**, *52* (8), 636−663.
(25) Chen, H.; Wu, J.; Zhu, X.; Ma, Y.; Li, Z.; Lu, L.; Aschner, M.; Su, P.; Luo, W. Manganese-induced miR-125b-2−3p promotes anxiety-like behavior via TFR1-mediated ferroptosis. *Environ. Pollut.* **2024**, *344*, 123255.
(26) Martins, A. C.; Krum, B. N.; Queirós, L.; Tinkov, A. A.; Skalny, A. V.; Bowman, A. B.; Aschner, M. Manganese in the Diet: Bioaccessibility, Adequate Intake, and Neurotoxicological Effects. *J. Agric. Food Chem.* **2020**, *68* (46), 12893−12903.
(27) Zhong, S.; Zhou, Q.; Yang, J.; Zhang, Z.; Zhang, X.; Liu, J.; Chang, X.; Wang, H. Relationship between the cGAS-STING and NF-κB pathways-role in neurotoxicity. *Biomed. Pharmacother.* **2024**, *175*, 116698.
(28) Ablasser, A.; Chen, Z. J. cGAS in action: Expanding roles in immunity and inflammation. *Science* **2019**, *363* (6431), aat8657.
(29) Chen, Q.; Sun, L.; Chen, Z. J. Regulation and function of the cGAS-STING pathway of cytosolic DNA sensing. *Nat. Immunol.* **2016**, *17* (10), 1142−1149.
(30) Motwani, M.; Pesiridis, S.; Fitzgerald, K. A. DNA sensing by the cGAS-STING pathway in health and disease. *Nat. Rev. Genet.* **2019**, *20* (11), 657−674.
(31) Sharma, M.; Rajendrarao, S.; Shahani, N.; Ramírez-Jarquín, U. N.; Subramaniam, S. Cyclic GMP-AMP synthase promotes the inflammatory and autophagy responses in Huntington disease. *Proc. Natl. Acad. Sci. U. S. A.* **2020**, *117* (27), 15989−15999.
(32) Yu, C. H.; Davidson, S.; Harapas, C. R.; Hilton, J. B.; Mlodzianoski, M. J.; Laohamonthonkul, P.; et al. TDP-43 Triggers Mitochondrial DNA Release via mPTP to Activate cGAS/STING in ALS. *Cell* **2020**, *183* (3), 636−649 e618.
(33) Xie, X.; Ma, G.; Li, X.; Zhao, J.; Zhao, Z.; Zeng, J. Activation of innate immune cGAS-STING pathway contributes to Alzheimer's pathogenesis in 5 × FAD mice. *Nat. Aging* **2023**, *3* (2), 202−212.
(34) Hooy, R. M.; Massaccesi, G.; Rousseau, K. E.; Chattergoon, M. A.; Sohn, J. Allosteric coupling between Mn^{2+} and dsDNA controls the catalytic efficiency and fidelity of cGAS. *Nucleic Acids Res.* **2020**, *48* (8), 4435−4447.
(35) Wang, C.; Guan, Y.; Lv, M.; Zhang, R.; Guo, Z.; Wei, X.; et al. Manganese Increases the Sensitivity of the cGAS-STING Pathway for Double-Stranded DNA and Is Required for the Host Defense against DNA Viruses. *Immunity* **2018**, *48* (4), 675−687 e677.
(36) Zhao, Z.; Ma, Z.; Wang, B.; Guan, Y.; Su, X. D.; Jiang, Z. Mn(2+) Directly Activates cGAS and Structural Analysis Suggests Mn(2+) Induces a Noncanonical Catalytic Synthesis of 2′3′-cGAMP. *Cell Rep.* **2020**, *32* (7), 108053.
(37) Eck, R. J.; Kow, R. L.; Black, A. H.; Liachko, N. F.; Kraemer, B. C. SPOP loss of function protects against tauopathy. *Proc. Natl. Acad. Sci. U. S. A.* **2023**, *120* (1), No. e2207250120.
(38) Wang, Y.; Mandelkow, E. Tau in physiology and pathology. *Nat. Rev. Neurosci.* **2016**, *17* (1), 22.
(39) Colom-Cadena, M.; Davies, C.; Sirisi, S.; Lee, J. E.; Simzer, E. M.; Tzioras, M.; et al. Synaptic oligomeric tau in Alzheimer's disease - A potential culprit in the sptad of tau pathology through the brain. *Neuron* **2023**, *111* (14), 2170−2183 e6.
(40) Maphis, N.; Xu, G.; Kokiko-Cochran, O. N.; Jiang, S.; Cardona, A.; Ransohoff, R. M.; Lamb, B. T.; Bhaskar, K. Reactive microglia drive tau pathology and contribute to the spreading of pathological tau in the brain. *Brain* **2015**, *138* (Pt6), 1738−1755.
(41) Wang, C.; Fan, L.; Khawaja, R. R.; Liu, B.; Zhan, L.; Kodama, L.; et al. Microglial NF-κB drives tau spreading and toxicity in a mouse model of tauopathy. *Nat. Commun.* **2022**, *13* (1), 1969.
(42) Forrest, S. L.; Lee, S.; Nassir, N.; Martinez-Valbuena, I.; Sackmann, V.; Li, J.; et al. Cell-specific MAPT gene expression is preserved in neuronal and glial tau cytopathologies in progressive supranuclear palsy. *Acta Neuropathol.* **2023**, *146* (3), 395−414.
(43) Khanna, M. R.; Kovalevich, J.; Lee, V. M.; Trojanowski, J. Q.; Brunden, K. R. Therapeutic strategies for the treatment of tauopathies: Hopes and challenges. *Alzheimers Dement.* **2016**, *12* (10), 1051−1065.
(44) Mummery, C. J.; Börjesson-Hanson, A.; Blackburn, D. J.; Vijverberg, E. G. B.; De Deyn, P. P.; Ducharme, S.; et al. Tau-targeting antisense oligonucleotide MAPT(Rx) in mild Alzheimer's

disease: a phase 1b, randomized, placebo-controlled trial. *Nat. Med.* **2023**, *29* (6), 1437−1447.
(45) Stamelou, M.; Respondek, G.; Giagkou, N.; Whitwell, J. L.; Kovacs, G. G.; Höglinger, G. U. Evolving concepts in progressive supranuclear palsy and other 4-repeat tauopathies. *Nat. Rev. Neurol.* **2021**, *17* (10), 601−620.
(46) Caballero, B.; Bourdenx, M.; Luengo, E.; Diaz, A.; Sohn, P. D.; Chen, X.; et al. Acetylated tau inhibits chaperone-mediated autophagy and promotes tau pathology propagation in mice. *Nat. Commun.* **2021**, *12* (1), 2238.
(47) Thibaudeau, T. A.; Anderson, R. T.; Smith, D. M. A common mechanism of proteasome impairment by neurodegenerative disease-associated oligomers. *Nat. Commun.* **2018**, *9* (1), 1097.
(48) Liu, J.; Zhang, X.; Ta, X.; Luo, M.; Chang, X.; Wang, H. Fecal microbiome transplantation attenuates manganese-induced neurotoxicity through regulation of the apelin signaling pathway by inhibition of autophagy in mouse brain. *Ecotoxicol. Environ. Saf.* **2022**, *242*, 113925.
(49) Chen, X.; Firulyova, M.; Manis, M.; Herz, J.; Smirnov, I.; Aladyeva, E.; et al. Microglia-mediated T cell infiltration drives neurodegeneration in tauopathy. *Nature* **2023**, *615* (7953), 668−677.
(50) Hammond, T. R.; Marsh, S. E.; Stevens, B. Immune Signaling in Neurodegeneration. *Immunity* **2019**, *50* (4), 955−974.
(51) Skopelja-Gardner, S.; An, J.; Elkon, K. B. Role of the cGAS-STING pathway in systemic and organ-specific diseases. *Nat. Rev. Nephrol.* **2022**, *18* (9), 558−572.
(52) Perl, D. P.; Olanow, C. W. The neuropathology of manganese-induced Parkinsonism. *J. Neuropathol. Exp. Neurol.* **2007**, *66* (8), 675−682.
(53) Krasemann, S.; Madore, C.; Cialic, R.; Baufeld, C.; Calcagno, N.; El Fatimy, R.; et al. The TREM2-APOE Pathway Drives the Transcriptional Phenotype of Dysfunctional Microglia in Neurodegenerative Diseases. *Immunity* **2017**, *47* (3), 566−581 e569.
(54) Shi, Y.; Manis, M.; Long, J.; Wang, K.; Sullivan, P. M.; Remolina Serrano, J.; Hoyle, R.; Holtzman, D. M. Microglia drive APOE-dependent neurodegeneration in a tauopathy mouse model. *J. Exp. Med.* **2019**, *216* (11), 2546−2561.
(55) Udeochu, J. C.; Amin, S.; Huang, Y.; Fan, L.; Torres, E. R. S.; Carling, G. K.; et al. Tau activation of microglial cGAS-IFN reduces MEF2C-mediated cognitive resilience. *Nat. Neurosci.* **2023**, *26* (5), 737−750.
(56) Li, X. D.; Wu, J.; Gao, D.; Wang, H.; Sun, L.; Chen, Z. J. Pivotal roles of cGAS-cGAMP signaling in antiviral defense and immune adjuvant effects. *Science* **2013**, *341* (6152), 1390−1394.
(57) Roy, E. R.; Wang, B.; Wan, Y. W.; Chiu, G.; Cole, A.; Yin, Z.; et al. Type I interferon response drives neuroinflammation and synapse loss in Alzheimer disease. *J. Clin. Invest.* **2020**, *130* (4), 1912−1930.
(58) Jack, C. R., Jr; Holtzman, D. M. Biomarker modeling of Alzheimer's disease. *Neuron* **2013**, *80* (6), 1347−1358.
(59) Ossenkoppele, R.; Schonhaut, D. R.; Schöll, M.; Lockhart, S. N.; Ayakta, N.; Baker, S. L.; et al. Tau PET patterns mirror clinical and neuroanatomical variability in Alzheimer's disease. *Brain* **2016**, *139* (Pt5), 1551−1567.
(60) Yuste-Checa, P.; Trinkaus, V. A.; Riera-Tur, I.; Imamoglu, R.; Schaller, T. F.; Wang, H.; et al. The extracellular chaperone Clusterin enhances Tau aggregate seeding in a cellular model. *Nat. Commun.* **2021**, *12* (1), 4863.
(61) Gui, X.; Yang, H.; Li, T.; Tan, X.; Shi, P.; Li, M.; Du, F.; Chen, Z. J. Autophagy induction via STING trafficking is a primordial function of the cGAS pathway. *Nature* **2019**, *567* (7747), 262−266.
(62) Menzies, F. M.; Fleming, A.; Caricasole, A.; Bento, C. F.; Andrews, S. P.; Ashkenazi, A.; et al. Autophagy and Neurodegeneration: Pathogenic Mechanisms and Therapeutic Opportunities. *Neuron* **2017**, *93* (5), 1015−1034.
(63) Tang, D.; Kang, R.; Berghe, T. V.; Vandenabeele, P.; Kroemer, G. The molecular machinery of regulated cell death. *Cell Res.* **2019**, *29* (5), 347−364.
(64) Wang, D.; Zhang, J.; Jiang, W.; Cao, Z.; Zhao, F.; Cai, T.; Aschner, M.; Luo, W. The role of NLRP3-CASP1 in inflammasome-mediated neuroinflammation and autophagy dysfunction in manganese-induced, hippocampal-dependent impairment of learning and memory ability. *Autophagy* **2017**, *13* (5), 914−927.
(65) Lachance, V.; Wang, Q.; Sweet, E.; Choi, I.; Cai, C. Z.; Zhuang, X. X.; et al. Autophagy protein NRBF2 has reduced expression in Alzheimer's brains and modulates memory and amyloid-beta homeostasis in mice. *Mol. Neurodegener.* **2019**, *14* (1), 43.
(66) Lee, J. H.; Yang, D. S.; Goulbourne, C. N.; Im, E.; Stavrides, P.; Pensalfini, A.; et al. Faulty autolysosome acidification in Alzheimer's disease mouse models induces autophagic build-up of Aβ in neurons, yielding senile plaques. *Nat. Neurosci.* **2022**, *25* (6), 688−701.
(67) Van Acker, Z. P.; Bretou, M.; Annaert, W. Endo-lysosomal dysregulations and late-onset Alzheimer's disease: impact of genetic risk factors. *Mol. Neurodegener.* **2019**, *14* (1), 20.
(68) Tammineni, P.; Ye, X.; Feng, T.; Aikal, D.; Cai, Q. Impaired retrograde transport of axonal autophagosomes contributes to autophagic stress in Alzheimer's disease neurons. *Elife* **2017**, *6*, No. e21776.
(69) Choi, I.; Wang, M.; Yoo, S.; Xu, P.; Seegobin, S. P.; Li, X.; et al. Autophagy enables microglia to engage amyloid plaques and prevents microglial senescence. *Nat. Cell Biol.* **2023**, *25* (7), 963−974.
(70) Xu, Y.; Propson, N. E.; Du, S.; Xiong, W.; Zheng, H. Autophagy deficiency modulates microglial lipid homeostasis and aggravates tau pathology and spreading. *Proc. Natl. Acad. Sci. U. S. A.* **2021**, *118* (27), No. e2023418118.
(71) Kabeya, Y.; Mizushima, N.; Ueno, T.; Yamamoto, A.; Kirisako, T.; Noda, T.; et al. LC3, a mammalian homologue of yeast Apg8p, is localized in autophagosome membranes after processing. *EMBO J.* **2000**, *19* (21), 5720−5728.
(72) Cassidy, L. D.; Narita, M. CELL BIOLOGY. GATA get a hold on senescence. *Science* **2015**, *349* (6255), 1448−1449.
(73) Liu, W. J.; Ye, L.; Huang, W. F.; Guo, L. J.; Xu, Z. G.; Wu, H. L.; Yang, C.; Liu, H. F. p62 links the autophagy pathway and the ubiqutin-proteasome system upon ubiquitinated protein degradation. *Cell Mol. Biol. Lett.* **2016**, *21*, 29.
(74) Tanji, K.; Miki, Y.; Ozaki, T.; Maruyama, A.; Yoshida, H.; Mimura, J.; et al. Phosphorylation of serine 349 of p62 in Alzheimer's disease brain. *Acta Neuropathol. Commun.* **2014**, *2*, 50.
(75) Wang, F.; Gómez-Sintes, R.; Boya, P. Lysosomal membrane permeabilization and cell death. *Traffic* **2018**, *19* (12), 918−931.
(76) Pajarillo, E.; Kim, S.; Digman, A.; Dutton, M.; Son, D. S.; Aschner, M.; Lee, E. The role of microglial LRRK2 kinase in manganese-induced inflammatory neurotoxicity via NLRP3 inflammasome and RAB10-mediated autophagy dysfunction. *J. Biol. Chem.* **2023**, *299* (7), 104879.
(77) Zhang, Z.; Yan, J.; Bowman, A. B.; Bryan, M. R.; Singh, R.; Aschner, M. Dysregulation of TFEB contributes to manganese-induced autophagic failure and mitochondrial dysfunction in astrocytes. *Autophagy* **2020**, *16* (8), 1506−1523.
(78) Sliter, D. A.; Martinez, J.; Hao, L.; Chen, X.; Sun, N.; Fischer, T. D.; et al. Parkin and PINK1 mitigate STING-induced inflammation. *Nature* **2018**, *561* (7722), 258−262.
(79) Congdon, E. E.; Wu, J. W.; Myeku, N.; Figueroa, Y. H.; Herman, M.; Marinec, P. S.; et al. Methylthioninium chloride (methylene blue) induces autophagy and attenuates tauopathy in vitro and in vivo. *Autophagy* **2012**, *8* (4), 609−622.
(80) Inoue, K.; Rispoli, J.; Kaphzan, H.; Klann, E.; Chen, E. I.; Kim, J.; et al. Macroautophagy deficiency mediates age-dependent neurodegeneration through a phospho-tau pathway. *Mol. Neurodegener.* **2012**, *7*, 48.
(81) Liu, D.; Wu, H.; Wang, C.; Li, Y.; Tian, H.; Siraj, S.; et al. STING directly activates autophagy to tune the innate immune response. *Cell Death Differ.* **2019**, *26* (9), 1735−1749.
(82) Prabakaran, T.; Bodda, C.; Krapp, C.; Zhang, B. C.; Christensen, M. H.; Sun, C.; et al. Attenuation of cGAS-STING signaling is mediated by a p62/SQSTM1-dependent autophagy pathway activated by TBK1. *EMBO J.* **2018**, *37* (8), No. e97858.

https://doi.org/10.1021/envhealth.4c00176
Environ. Health 2025, 3, 199−212

(83) Liu, C.; Yan, D. Y.; Wang, C.; Ma, Z.; Deng, Y.; Liu, W.; Xu, B. Manganese activates autophagy to alleviate endoplasmic reticulum stress-induced apoptosis via PERK pathway. *J. Cell. Mol. Med.* **2020**, *24* (1), 328−341.
(84) Zhang, X.; Wei, M.; Fan, J.; Yan, W.; Zha, X.; Song, H.; et al. Ischemia-induced upregulation of autophagy preludes dysfunctional lysosomal storage and associated synaptic impairments in neurons. *Autophagy* **2021**, *17* (6), 1519−1542.

https://doi.org/10.1021/envhealth.4c00176
Environ. Health 2025, 3, 199−212